ACS APPLIED MATERIALS & INTERFACES

Research Article

www.acsami.org

Spectroscopic Ellipsometry Analysis of a Thin Film Composite Membrane Consisting of Polysulfone on a Porous α-Alumina Support

Wojciech Ogieglo,[†] Herbert Wormeester,[‡] Matthias Wessling,[†,⊥] and Nieck E. Benes*[,§]

[†]Membrane Science and Technology, [‡]Physics of Interfaces and Nanomaterials, [§]Inorganic Membranes, Department of Science and Technology and MESA+ Institute for Nanotechnology, University of Twente, P.O. Box 217, 7500 AE Enschede, The Netherlands

ABSTRACT: Exposure of a thin polymer film to a fluid can affect properties of the film such as the density and thickness. In particular in membrane technology, these changes can have important implications for membrane performance. Spectroscopic ellipsometry is a convenient technique for in situ studies of thin films, because of its noninvasive character and very high precision. The applicability of spectroscopic ellipsometry is usually limited to samples with well-defined interfacial regions, whereas in typical composite membranes, often substantial and irregular intrusion of the thin film into the pores of a support exists. In this work, we provide a detailed characterization of a polished porous alumina membrane support, using variable-angle spectroscopic ellipsometry in combination with atomic force microscopy and mercury porosimetry. Two Spectroscopic ellipsometry optical models are presented that can adequately describe the surface roughness of the support. These models consider the surface roughness as a distinct layer in which the porosity gradually increases toward the outer ambient interface. The first model considers the porosity profile to be linear; the second model assumes an exponential profile. It is shown that the models can be extended to account for a composite membrane geometry, by deposition of a thin polysulfone film onto the support. The developed method facilitates practicability for in situ spectroscopic ellipsometry studies of nonequilibrium systems, i.e., membranes under actual permeation conditions.

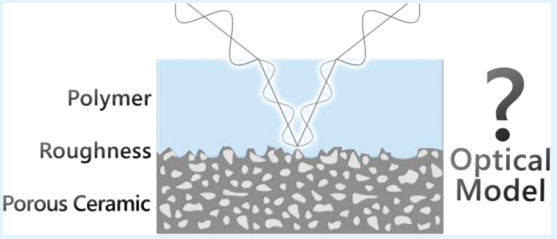

KEYWORDS: *spectroscopic ellipsometry, thin film composite membranes, surface roughness, porous support, alumina, polysulfone*

1. INTRODUCTION

Thin films are widely used in many areas of science and technology, serving as coatings[1] or membranes,[2,3] and for the fabrication of sensors[4] and microelectronic devices.[5] Application areas of thin films often involve their use as an interface between fluid phases with different thermodynamic status. For instance, in membrane technology, molecular selectivity is often provided by a thin film serving as semipermeable barrier. Separation performance of such a thin selective film is strongly dependent on penetrant concentration profiles inside film. These profiles are in turn dictated by the interactions between the thin film and the fluid mixtures it separates. In the case of polymer membranes, penetrant-induced sorptive dilation or swelling[6] may significantly change the molecular structure and macromolecular dynamics of the material. For instance, in gas separation, large concentrations of highly interacting penetrants can be responsible for undesired plasticization phenomena, thereby limiting the window of membrane operation.[3,7] Fundamental understanding of such penetrant induced phenomena will aid membrane material choice and optimization of process parameters.

The majority of commercial membranes have an asymmetric composite geometry, comprising a thin selective film deposited on a highly porous support.[3] The support and the film can be organic[8] as well as inorganic.[9] Characterization of supported thin films can be accurately performed with many techniques, including Brillouin light scattering,[10] particle embedding,[11] dielectric relaxation spectroscopy,[12,13] buckling instability,[14] positron annihilation spectroscopy,[15] X-ray photon correlation spectroscopy,[16] and spectroscopic ellipsometry.[17,18] Few of these techniques have been applied for in situ characterization of thin films exposed to a penetrant.[8,12,17,19−21] For example, for thin films in contact with liquid or gaseous penetrant in situ spectroscopic ellipsometry allows determination of the swelling degree and the estimation of the concentration of the dissolved penetrant.[18] Such in situ spectroscopic ellipsometry analyses are normally limited to equilibrium conditions, when the films are supported on nonporous substrates such as silicon wafers or glass slides. In actual membrane applications the film separates two phases that are not in thermodynamic equilibrium, and mass transport occurs from one side of the film to the other. This requires the layer that supports the thin selective film to be very permeable, i.e., highly porous. Typically, however, porosity introduces roughness in the sample structure which makes the ellipsometry analysis difficult due to diffuse light scattering or depolarization effects. Moreover, if the interface between the dense skin and the porous support of the membrane is not well-defined (i.e., pore intrusion) the interpretation of ellipsometry parameters, Psi and Delta, may be hindered. To characterize thin membrane films in realistic membrane application conditions, we will need to extend the in situ spectroscopic ellipsometry approach to account for porous substrates.

Received: November 15, 2011
Accepted: January 12, 2012
Published: January 12, 2012

The purpose of this work is to study the applicability of in situ spectroscopic ellipsometry in investigations involving composite flat disk membranes, in which a ceramic porous support is covered with a thin polymer film. The support chosen here is a very well-defined, chemically and mechanically stable porous alumina material characterized by uniform roughness. On the alumina support, a thin polysulfone (PSU) film is deposited by floating technique, which minimizes the polymer pore intrusion. For the sample designed in such a way, a viable spectroscopic ellipsometry model is provided.

2. SPECTROSCOPIC ELLIPSOMETRY PRINCIPLES

Spectroscopic Ellipsometry is a nondestructive optical technique that allows very precise in situ analysis of the properties of thin films. Combined with appropriate data analysis and modeling, spectroscopic ellipsometry can yield information on the film thickness and refractive index.

In spectroscopic ellipsometry, light of a well-defined polarization state (usually linearly polarized) is reflected of a thin film−substrate system. The reflection results in the change of the polarization state of light, in general into elliptically polarized. The parameters that describe the change of the polarization state upon reflection are psi (Ψ) and delta (Δ), which are defined in eq 1.

$$\tan(\Psi)e^{i} = \rho = \frac{r_p}{r_s} \tag{1}$$

The symbols r_p and r_s refer to reflectivity of p and s polarized light, respectively. For further details on the basics of ellipsometry, the reader is referred to one of the handbooks.[22,23]

The measured psi and delta are collected over a range of wavelengths of light. Extracting meaningful physical information from this ellipsometric spectrum requires the construction of an optical model of the sample. In general, this optical model takes into account a number of distinct layers with individual optical dispersions. Interfaces between these layers are optical boundaries at which light is refracted and reflected according to the Fresnel relations. The total reflected light is a product of constructive and destructive interferences of light rays reflected from all of the optical interfaces. The psi and delta values generated for a given optical model are numerically matched to the measured psi and delta, by adjusting the values of fitting parameters. Fitting parameters can include the thickness, the real part of the refractive index n (or the optical dispersion) and the imaginary part of the refractive index k (extinction coefficient) of the different layers. In the case of weakly or nonabsorbing dielectric materials, the extinction coefficient is close to zero and the optical dispersion can be successfully fitted to the well-known Cauchy dispersion (eq 2):

$$n(\lambda) = A + \frac{B}{\lambda^2} + \frac{C}{\lambda^4} \tag{2}$$

The difference between the optical response predicted by an optical model and the measured data (the quality of fit) can be expressed by the mean square error (MSE). The MSE is defined as the square root of the sum of errors between the measured and model generated values. The lower the value of the MSE, the closer the data generated from a model are to the measured data. Generally, it is considered that an MSE value between 1 and 2 describes a good fit for single angle of incidence of incoming light and layer thickness in the range 100−200 nm. For thicker layers, higher values of MSE are considered acceptable. For thicker layers, ellipsometry spectra display more oscillations; at the same measurement resolution, less measured values describe the single oscillation in case of a thicker film as compared to a thin film. In analogy, higher MSE values are considered acceptable for ellipsometry spectra with much structure in the measured data. The MSE value is also expected to be higher when analysis is performed simultaneously on spectra taken at multiple angles of incidence, because of error accumulation (angle of incidence determination accuracy, beam collimation etc.).

The layer thickness range that can be determined by ellipsometry matches well with the typical thickness range of selective membrane skin layers (30−2000 nm).[2,24,25] However, a crucial requirement for spectroscopic ellipsometry is that the support layer beneath the studied thin film needs to be very well-defined and uniform. Typical substrates include polished silicon wafers, glass slides, or metallic discs. If the substrate surface features dimensions exceed ∼30% of the wavelength of the probing light, pronounced scattering effects occur that may strongly complicate analysis.[22] This requirement is very rarely met in asymmetric or composite membranes where the support pore dimensions are often much larger than this limit.

In addition to light scattering by pores in the support layer, ellipsometry is also complicated by large surface roughness or pronounced thickness variations. Such sample nonidealities result in a partial depolarization of the reflected light, which can significantly increase the errors of the analysis. For instance, if the analyzed sample is characterized by large surface roughness some portion of the probing light will be scattered (multiply reflected) on the surface. That will result in a different polarization state as compared to the light reflected from the sample surface only once. Similarly, if the thin film deposited on the substrate is nonuniform with respect to its thickness, light reflected from such a sample carries different polarization state depending on the lateral position of the light ray reflection. Other physical phenomena responsible for depolarization include incident angle or wavelength variations and are related to the characteristics of the experimental setup. The intensity of reflected light also affects modeling quality, as the polarization state of light is determined from the light intensity. Thus, severe reduction in light intensity upon reflection complicates ellipsometry analysis.

The optical properties of a mix of materials can be approximated using an effective medium approximation (EMA) theory. EMA theories are based on the assumption that the mean optical dispersion of a medium which comprises of two different dielectric substances can be approximated by mixing their dielectric constants or, using the relationship $\varepsilon = n^2$, their refractive indices (n_a and n_b), for instance, according to the formula proposed by Bruggeman (eq 3):

$$f_a \frac{n_a^2 - n_{eff}^2}{n_a^2 + 2n_{eff}^2} + (1 - f_a)\frac{n_b^2 - n_{eff}^2}{n_b^2 + 2n_{eff}^2} = 0 \tag{3}$$

where f_a is the volume fraction of the substance a and n_{eff} is the effective refractive index. Bruggeman approach, therefore, makes the self-consistent choice of the host material where the polarizability of the intruded material is related to the polarizability of the host. In this way the porosity of a material can be represented as a mix of void refractive index ($n = 1$) and refractive index of dense material. The EMA approach can also be used to approximate the concentration of a penetrant in a polymer matrix for instance treating the dissolved substance as a liquid phase homogeneously mixed with host on a molecular level.[8,18]

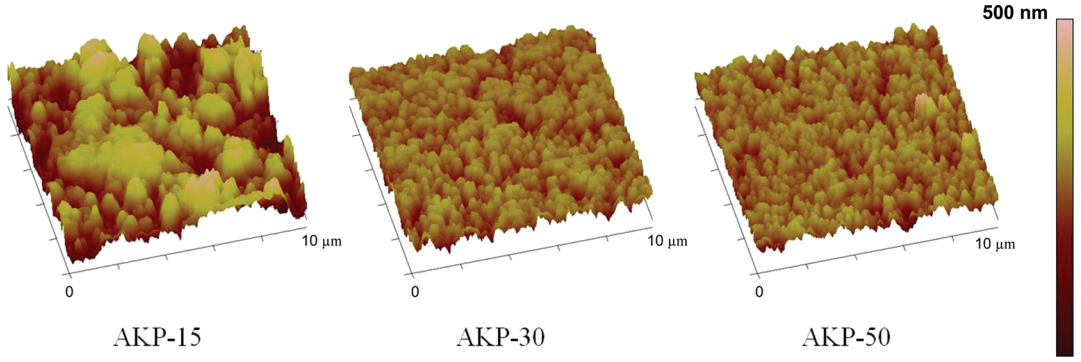

Figure 1. AFM topology images for AKP-15, AKP-30, and AKP-50 samples, vertical (out of plane) height scale relates to all three topology maps.

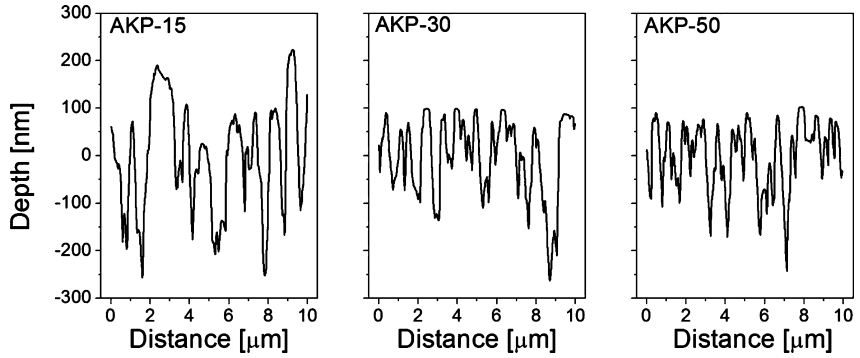

Figure 2. Representative AFM line scans over 10 μm distances of the surface.

Complex optical models can be devised in an attempt to account for the effects of thickness nonuniformity, surface roughness, refractive index gradients, and materials mixing.

3. EXPERIMENTAL SECTION

3.1. Materials. Alpha alumina porous disks were prepared form commercial alumina powders: AKP-15, AKP-30 and AKP-50 (Sumitomo Chemical, Japan) with average particle size of 0.7 μm, 0.3 μm, and 0.2 μm, respectively. Commercial polysulfone (PSU) Udel P-3500 (Amoco, Solvay Advanced Polymers) and cyclopentanone (Sigma Aldrich) were used as received. Three mm thick glass slides prepared in house were used for the PSU free-standing film preparation.

3.2. Support Preparation. The alpha alumina supports in a flat disk geometry were prepared according to the protocol described in detail elsewhere.[26] The procedure involved the preparation of the AKP owder suspension in an acidic solution with the addition of poly(vinyl acetate) (PVA). A green compact was obtained by filtering the suspension in a mold. After sintering at 1100 °C the obtained disk was cut to the desired dimensions, and one surface was polished mechanically to produce a smooth interface.

3.3. Layer Deposition. A solution of 10%wt PSU in cyclopentanone was spin coated on a clean glass slide, followed by annealing for 5 h at 120 °C under nitrogen flow in order to remove the remaining solvent. The glass slide with film was then immersed in deionised water, causing it to dewet and float on the surface within 1 h. The free-standing film was gently placed on top of a AKP-50 support and dried in a furnace at 100 °C for 1 h under nitrogen flow. Subsequently, the furnace temperature was increased to 250 °C (PSU T_g =185 °C) for 2 h to accomplish partial intrusion of the polymer into the surface roughness of the alumina support, ensuring a good adhesion of the film. Samples prepared in this way were then quenched to room temperature by removing them from the furnace, and used for spectroscopic ellipsometry analysis.

3.4. Characterization. *3.4.1. Atomic Force Microscopy (AFM).* Atomic force microscopy imaging was performed with a Dimension 3100 AFM equipped with a hybrid scanner and NanoScope Iva controller (Veeco/Digital Instruments, Santa Barbara, CA, USA) operated in a tapping mode. Commercially available silicon cantilevers (PointProbe Plus silicon probes, PPP-NCH, Nanosensors, Neuchatel, Switzerland) were used.

3.4.2. Spectroscopic Ellipsometry. Spectroscopic ellipsometry measurements were performed with two systems, both supplied by J.A. Woolam Co., Inc. A rotating compensator ellipsometer (M-2000X) was used for the UV−vis range of the spectrum 210−1000 nm. The M-2000X is characterized by fast acquisition times: less than 10 s per single incident angle. The second system, a rotating analyzer ellipsometer (VASE), was used to probe the samples in the near-infrared, up to about 1700 nm. The combined range of wavelengths available for analysis was 210−1700 nm. The spot size of the probing light had a diameter of 2 mm in case of both spectroscopic ellipsometers used. The spectral resolution for the M-2000X and the VASE ellipsometers was 2 and 5 nm, respectively, which was high enough to adequately capture psi and delta oscillations of the polymer deposited sample. For all samples measurements were conducted at multiple angles of incidence, to improve reliability of data interpretation and modeling. Data modeling was performed with a commercial software package (Complete EASE v.4.41) supplied with the M-2000X system.

The thickness and optical constants of the PSU film deposited on glass were determined with the M-2000X, assuming using simple Cauchy dispersions for the glass substrate and the polymer film. First, the pure glass substrate was analyzed, accounting for surface roughness on the nanometer scale. The derived optical constants were kept fixed in the subsequent analysis of the supported PSU layer. Second, the thin supported PSU layer was characterized, yielding thickness (1115 nm) and Cauchy optical dispersion function with $n_{632.8\ nm}$ = 1.625. The dispersion function was assumed the same after deposition onto the alpha alumina porous support.

3.4.3. Mercury Porosimetry. Porosity of all the samples was determined with a mercury PoreMaster porosimeter (Quantachrome).

4. RESULTS AND DISCUSSION

4.1. Characterization of the Alpha Alumina Disks. *4.1.1. Atomic Force Microscopy.* The Atomic force

dx.doi.org/10.1021/am2015958 | ACS Appl. Mater. Interfaces 2012, 4, 935−943

microscopy topography images of polished flat disk samples of AKP-15, AKP-30, and AKP-50 are presented in Figure 1. In each case the scan area presents a square region of 10 μm × 10 μm. The surfaces of AKP-30 and AKP-50 disks exhibit surface roughness features of a comparable size. In the case of AKP-15, the surface roughness features are much larger and surface morphology is significantly more irregular.

More precise analysis of the topmost roughness layer is performed based on depth line scans over a distance of 10 μm (Figure 2) and their corresponding cumulative height distributions (Figure 3). In Figure 2, the zero value on the *Y*-axis

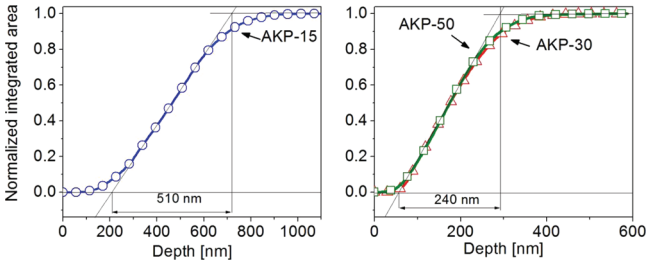

Figure 3. AFM cumulative height distribution for AKP-15, AKP-30, and AKP-50; symbols are guides for the eyes.

represents the average depth of the sample features as determined for the whole analyzed area. AKP-30 and AKP-50 types are relatively uniform over the area analyzed, as is indicated by only slightly asymmetric bell-shaped line scan histograms (not shown). In the case of AKP-15 the line scan histogram presents a much wider, though also symmetric shape.

Correlation analysis of the AFM images reveals the average sizes of the surface roughness features to be 370, 170, and 160 nm for the AKP-15, AKP-30, and AKP-50, respectively.

In Figure 3, the AKP-30 and AKP-50 profiles nearly completely coincide. The corresponding profiles of the cumulative height distribution show an almost linear increase of the void fraction, going from the uniform bulk of the sample outward. The depth over which the increase occurs can be quantified by a simple tangent construction as indicated in Figure 3. In the case of AKP-15, the range over which the void fraction changes reaches 510 nm ,which is approximately two times more than in the case of AKP-30 and AKP-50 (240 nm).

4.1.2. Spectroscopic Ellipsometry. Figure 4 combines the measurements of signal intensity and depolarization of light

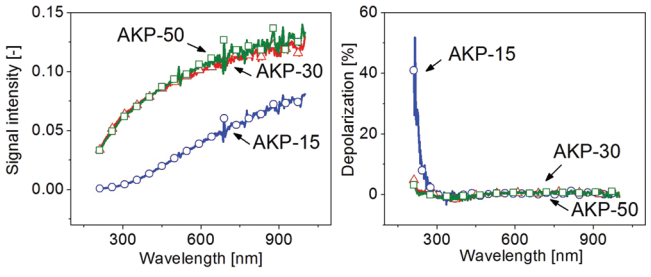

Figure 4. Signal intensity and depolarization of light for AKP-15, AKP-30, and AKP-50 disks measured with a 2 mm light spot size at 70° angle of incidence; symbols are guides for the eyes.

reflected at 70° angle of incidence as a function of light wavelength, for three support types. In all cases, the light intensity decreases for shorter wavelengths. This is probably related to more pronounced scattering as the wavelength approaches the scale of sample surface roughness features. In the case of AKP-15 the reflected signal is much weaker than in the case of AKP-30 and AKP-50 and vanishes completely below about 300 nm.

In the visible range, depolarization is very low for all measured samples. Only for AKP-15 a sharp decrease in depolarization is observed below 300 nm. This is in a good agreement with the much larger scale of surface irregularities of the AKP-15, and is related to significant scattering at shorter wavelengths.

Table 1 shows, for the three sample types, the mean value and standard deviation (SD) of psi (at 632.8 nm, 70° angle of

Table 1. Measured Mean Psi Values at 632.8 nm Wavelength Together with Calculated Standard Deviation (SD) from 10 Different Spots on AKP-15, AKP 30 and AKP-50, Instrumental SD in Psi Determination, and Particle Grain Size Used for the Preparation of the Samples

sample	mean psi at 632.8 nm	SD of psi from 10 spots at 632.8 nm	instrumental SD of psi at 632.8 nm	particle grain size (μm)
AKP-15	28.8	0.8	0.03	0.7
AKP-30	28.5	0.3	0.02	0.3
AKP-50	28.34	0.05	0.02	0.2

incidence) for 10 measured spots across a sample surface, and the instrumental SD in psi determination. The instrumental SD is largest for AKP-15 For all samples the instrumental SD is much less than the spot to spot SD, indicating that nonuniformity can be assessed with higher accuracy than the experimental error. The results show that the spot to spot nonuniformity increases strongly with increasing grain size. Apparently, surface polishing of the alumina supports made with smaller particles results in much more uniform surface roughness features. In accordance, AKP-50 samples are characterized by the highest uniformity of surface roughness.

For AKP-30 and AKP-50, the sufficient signal intensity, the low depolarization, and uniform surface features indicate that it may be possible to construct an appropriate optical model for interpretation of ellipsometry data.

4.2. Spectroscopic Ellipsometry Model Development. *4.2.1. Uncoated Alumina Support.* Constructing an appropriate optical model is facilitated by investigating the behavior of the so-called pseudo optical transforms $\langle n \rangle$ and $\langle k \rangle$, especially with respect to dependence on angle of incidence. As defined in (eq 4) $\langle n \rangle$ and $\langle k \rangle$ are directly related to the measured psi and delta values.

$$(\langle n \rangle + i\langle k \rangle)^2 = \sin(\varphi)^2\left[1 + \tan(\varphi)^2\left(\frac{1-\rho}{1-\rho}\right)^2\right] \quad (4)$$

Pseudo optical transformation of multiangle spectroscopic data is useful in order to gain some basic information about the sample structure. If the analyzed sample morphology is isotropic and comprises only a single optical interface, for instance in the case of a bare polished substrate, the pseudo optical constants are independent of the angle of incidence and are equivalent to the materials actual optical constants *n* and *k*. If the pseudo optical constants are angle-dependent, the sample can be represented more appropriately by an anisotropic or a multilayer structure. This is for instance typical for samples possessing oxide layers, thin films, roughness, or complex anisotropic geometry.[27]

dx.doi.org/10.1021/am2015958 | ACS Appl. Mater. Interfaces 2012, 4, 935–943

The pseudo optical constants for an AKP-30 sample, for angles of incidence 65°, 70° and 75°, are depicted in Figure 5.

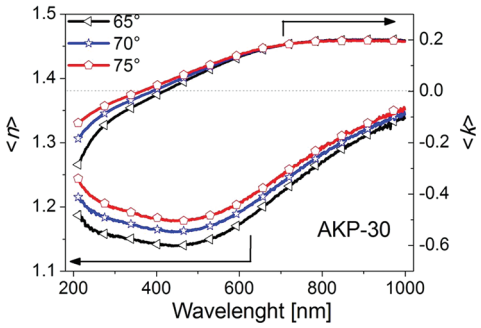

Figure 5. Pseudo transforms ⟨*n*⟩ and ⟨*k*⟩ for AKP 30 at angles of incidence of 65, 70, and 75°; symbols are guides for the eyes.

The results are representative also for AKP-15 and AKP-50, and show a significant dependence of the pseudo transforms on angle of incidence. Additionally, the ⟨*k*⟩ values show unphysical negative values at wavelengths below about 450 nm. This strongly suggests that the samples do not possess a single isotropic interface structure. An appropriate optical model for such samples should involve a multilayer system or anisotropy.

On the basis of the conclusions from the atomic force microscopy and ellipsometry analysis, it seems reasonable to treat the surface roughness of the alumina supports as a separate layer with graded porosity. The corresponding model is schematically presented in Figure 6 and involves the use of the Bruggeman

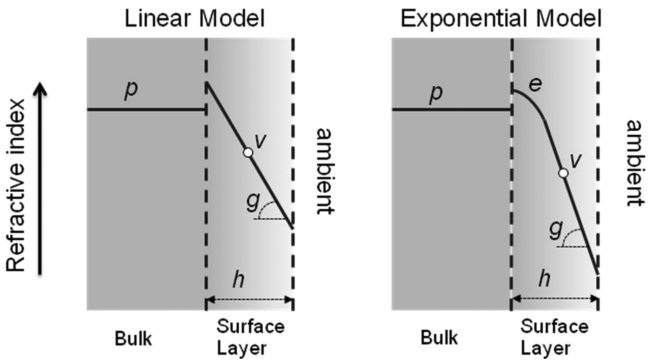

Figure 6. Schematic representation of the ellipsometric models for AKP materials.

EMA for mixing the optical constants of two components. The first component is dense alumina, represented by a fit of the Cauchy equation to optical dispersion data of corundum—Al_2O_3 taken from literature.[28] The calculated parameters are $A = 1.751$, $B = 6.32 \times 10^{-3}$, $C = 1.0152 \times 10^{-5}$ and produce the value of refractive index of $n_{Al2O3} = 1.766$ at 632.8 nm. The other component is void, representing the porosity of the porous alumina structure, with $n_{void} = 1.000$ over the whole wavelength range.

The optical model comprises two materials distributed over two distinct optical layers. The bottom layer, bulk, consists of porous alumina with a constant void fraction *p*. This void fraction is used as fitting parameter and the value obtained from the fit is expected to agree with the results of mercury porosimetry measurements (~40%).

The top layer, surface layer, consists of porous alumina with decreasing void fraction, going from the interface with the bottom layer toward the outer surface (the interface with the ambient). The thickness of the layer (*h*) is considered a fitting parameter in the optical model. For each position in the layer, the local void fraction can be transformed into the refractive index using the Bruggeman EMA. For this, the optical model requires an expression for the spatial variation in void fraction. In this study, two expressions are proposed. The first expression considers the void fraction to be a linear function of the depth (linear model). This expression contains two adjustable fit parameters: the gradient in void fraction *g*, and the void fraction in the middle of the film *v*. The second expression considers the refractive index to be an exponential function of the depth (exponential model). This expression is expected to be able to account for the curvature of the density profile closer to the support, visible between 250 and 400 nm in Figure 3. In the exponential model, in addition to *g* and *v*, the exponent *e* is an adjustable fitting parameter. Importantly, the values of refractive indices corresponding to porosity of the surface layer at the bulk interface are not coupled to those related to the porosity of the bulk support. This is done in order to test whether the model is able to reproduce the index profile in a physically consistent way (i.e., more or less continuous index profile) without introducing any initial restrictions.

The void profiles obtained from the ellipsometry analysis should correspond with the cumulative height distributions from AFM analysis (Figure 3). Bruggeman EMA is therefore used to transform the mass density profile obtained from AFM directly into the profile of refractive index. The bulk value of support refractive index is calculated on the basis of the known refractive index and density of dense alpha alumina which are $n_{Al2O3} = 1.766$ at 632.8 nm and $\rho_{Al2O3} = 4.0$ g cm^{-3}, respectively. The porosity of the samples is taken from mercury porosimetry measurements and indicated in Table 2. The AFM reference profile prepared in this way is thus completely independent from the ellipsometric measurements.

Representative fit results for Psi in the wavelength range 450−1000 nm and 5 angles of incidence are shown in Figure 7, for both the Linear Model and the Exponential Model. Visual inspection of the spectra suggests a proper fit for both models, as is confirmed by the low MSE (~7) obtained with both models. The same is also true for the Delta parameter that is not shown for the sake of clarity. The fit quality decreases at lower wavelengths, especially for smaller angles of incidence. This is probably an effect of more pronounced scattering.

To reduce the negative effects of scattering and to concurrently improve reliability of the fit, we omitted smaller wavelengths in the fitting procedure. The lower limit of the wavelength range is determined from a maximum value allowed for the MSE. The criterion in case of AKP-30 and AKP-50 was an MSE lower than an arbitrary value of about 5, for simultaneous fit for all angles of incidence. This value indicates a very good fit quality considering the simultaneous fit to 5 sets of data. Fit results for all investigated materials using both Linear and Exponential models, and the wavelength range used for the fit are collected in Table 2. In the case of AKP-15, the wavelength range was confined to the NIR range, due to large experimental uncertainties caused by low signal intensity and scattering effects in the UV and visible range. For AKP-15, even in the IR range the MSE obtained is still high (MSE = 16) and the models are considered poorly applicable.

In Figure 8, the generated refractive index profiles for the linear model and exponential model are compared with the AFM-derived refractive index profile, for an AKP-50 support.

dx.doi.org/10.1021/am2015958 | ACS Appl. Mater. Interfaces 2012, 4, 935−943

Table 2. Model Fitting Results for AKP-15, AKP-30, and AKP-50 Flat Disc Samples

model	sample	wavelength range	thickness of top layer, h (nm)	mean void fraction in the top layer, v (%)	gradient in the top layer, g (%)	exponent, e	porosity of the support, p (%)	porosity of the support from Hg porosimetry (%)	average pore diameter (nm)
linear	AKP 50	525−1700 MSE = 5	198.9 ± 0.4	56.0 ± 0.06	71.6 ± 0.1		39.7 ± 0.1	41.9	78
	AKP 30	560−1700 MSE = 5	212.6 ± 1	49.8 ± 0.1	75.7 ± 0.4		33.8 ± 0.1	35.6	74
	AKP 15	1200−1700 MSE = 16	307 ± 15	56.2 ± 0.7	23.3 ± 5.5		41.5 ± 0.9	42.4	130.6
exponential	AKP 50	550−1700 MSE = 5.2	318.6 ± 3.7	76.1 ± 0.1	104.1 ± 0.3	2.01 ± 0.04	37.0 ± 0.2	41.9	78
	AKP 30	600−1700 MSE = 5.2	370.2 ± 2.8	75.7 ± 0.04	119.4 ± 0.4	2.50 ± 0.04	31.0 ± 0.2	35.6	74
	AKP 15	1200−1700 MSE = 14.8	296 ± 11	78 ± 11	56 ± 19	13.1 ± 1.8	42.0 ± 0.8	42.4	130.6

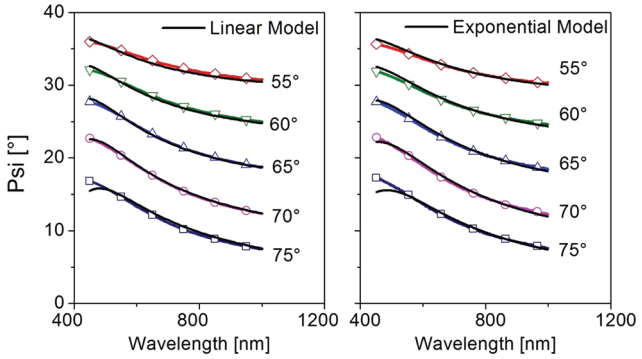

Figure 7. Measured and fit generated values of Psi for AKP-50 sample over the wavelength range 450−1000 nm for angles of incidence of 55, 60, 65, 70, 75°. Both linear and exponential models are presented. Symbols are guides for the eyes.

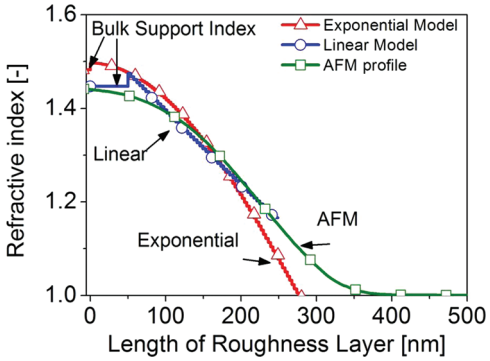

Figure 8. Generated refractive index profile compared with the void−alpha alumina profile obtained from the integrated histogram AFM analysis; symbols are guides for the eyes.

The refractive index profile predicted by both models is in good agreement with the profile obtained with AFM. For both models, the refractive index of bulk corresponds to porosity (p) comparable with that obtained via mercury intrusion. The thickness of the graded layer (surface layer) obtained from the optical models (h) and the AFM data are in good agreement. The refractive index at the interface between the two layers is more or less continuous, and the average value (v) and slope (g)/shape (e) of the refractive index is similar to that derived from AFM. It is important to mention that all fit parameters are fitted simultaneously, with no restrictions imposed on their values. The physically realistic values that are obtained indicate that the models are reliable, robust and stable. Comparable conclusions hold for AKP-30.

The thickness of surface layer obtained from the linear model is smaller as compared to the exponential model. It can be rationalized by the consideration that the linear model tends to represent better the linear part of the AFM profile, which is located in the middle of the surface layer. The curvature of the density profile in between the bulk and the linear part of the AFM profile cannot be captured adequately by the linear model. Instead, this nonlinear region in the density profile is considered part of bulk, resulting in a lower value for the thickness h.

The exponential model estimates a slightly larger value for the thickness h, and generates a refractive index smaller than 1 at the ambient interface. This model tends to match the shape of the nonlinear variation in density close to Bulk, and at the same time tends to match the linear shape in the region closer to sample surface. In this way, the exponential model includes this nonlinear density variation in surface layer, whereas this region is considered part of bulk in the linear model. Consequently, the exponential model predicts a larger overall thickness of the surface layer as compared to the linear model. Because only a single parameter e is available, the exponential model is forced to consider a linear variation of refractive index at the interface with the ambient. This is physically unrealistic and results in the nonphysical value of the refractive index at the ambient interface. Additionally, refractive index overestimation at the Bulk interface is produced by the exponential model. Because the MSE values obtained for both models in a similar wavelength range are very close together ($MSE_{LinearModel}$ = 5.0 and $MSE_{ExponentialModel}$ = 5.2), it is difficult to discern which one is more appropriate.

Overall, it can be concluded that the most consistent and robust results are obtained in the case of AKP-30 and AKP-50, for both types of models. The wavelength range of the fit with an MSE of about 5 is the largest in the case of AKP-50.

4.2.2. PSU Layer Deposited on Alpha Alumina Support−Preliminary Model. The models can be extended to account for composite membrane geometry: a thin dense film on top of the support with surface roughness. We have selected AKP-50 as support, given conclusions from the AFM and ellipsometry characterization of the three support types investigated, and polysulfone as material for the dense thin film, because of the wide application of this polymer in the membrane science and technology. AKP-50 was chosen over AKP-30 due to its best-fit quality, widest applicable wavelength range, and higher reflected light intensity. For AKP-15 the combination of high

dx.doi.org/10.1021/am2015958 | ACS Appl. Mater. Interfaces 2012, 4, 935−943

MSE, much narrower applicable wavelength range (only NIR), lower intensity (Figure 4) and moderate agreement with the AFM profile would make the analysis of a composite sample much more difficult and less relevant for the intended application. The approach is not limited to polysulfone; for other polymers sample preparation, post treatment, and modeling can be similar, provided that the polymer can dewet from a glass slide during immersion in solvent. That is because most typical high T_g polymers have their refractive indices in the range between ~1.55 and 1.65, which is close to that of the polymer applied in this study (1.625).

The optical model for the alumina support with thin polymer layer comprises three distinct layers, as shown schematically in Figure 9. In this model, referred to as multilayer model,

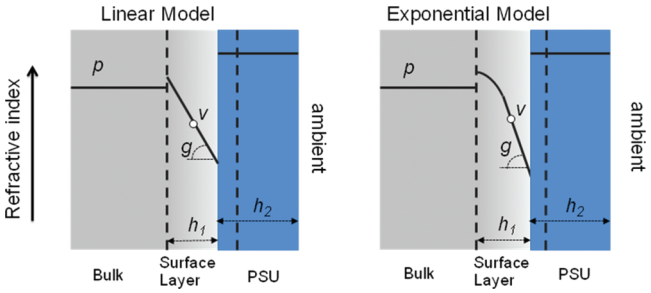

Figure 9. Schematic of the models for thin PSU layer deposited on AKP-50.

essentially the two-component geometry of the AKP-50 support is extended with an additional PSU layer. This layer accommodates a thin region in which the polymer is intruding the porous alumina. This intrusion layer comprises predominantly PSU, a small fraction of dense alumina and presumably a very small fraction of void. The difference in refractive indices of PSU and dense alumina is not very large (n_{PSU} = 1.625 and n_{Al2O3} = 1.766; both with typical Cauchy dispersion and negligible extinction coefficients in the analyzed wavelength range). Assuming an alumina volume fraction of 15% in the intruded region, the index of the intrusion layer can be calculated to be approximately n_{Intr} = 1.646. Considering that the value is very close to the index of pure PSU and that the intrusion layer is estimated to be an order of magnitude thinner than the total thickness of the deposited film, the refractive index of this intrusion region is assumed identical to that of pure PSU. This assumption avoids the introduction of a fourth layer in the optical model, which would significantly complicate data analysis. The optical dispersion of the PSU Cauchy layer is taken from the ellipsometry results for PSU layer deposited on glass. For the AKP-50 support, the linear model or exponential model can be used to describe the variation in void fraction. In the case of the exponential model, the curvature (exponent fit parameter, e) was first determined from bare AKP-50 and then held fixed. Also the void fraction of the bulk alpha alumina substrate (p) is determined from bare AKP-50 and held fixed. These assumptions are considered viable and substantially decrease the amount of fit parameters in the multilayer model for the deposited sample.

The remaining fit parameters in the Multilayer Model are the thickness of the PSU layer (comprising the intrusion region) h_2, thickness of the remaining roughness layer h_1, and the average value v and gradient g of the void fraction of the remaining roughness layer. For both models the refractive index profiles are presented in Figure 10, together with the profile obtained from AFM for reference. Figure 11 shows the fit to psi and

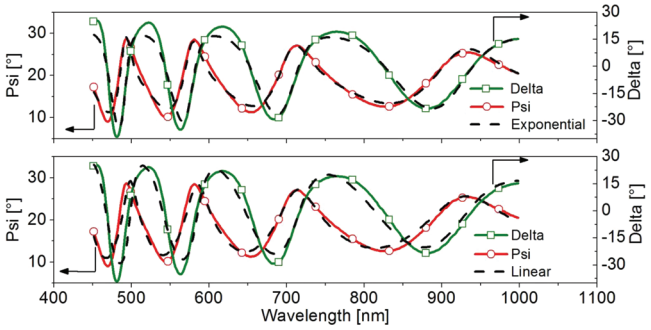

Figure 11. Psi and delta fit results of the multilayer models for ~1100 nm PSU layer deposited on AKP-50 based on the exponential model.

delta parameters measured for the coated sample. The model fitting is performed in the wavelength range of 450−1000 nm and with angle of incidence of 70°.

The model fitting results are also presented in Table 3. For both models, the MSE value is relatively high (exponential MSE = 33, linear MSE = 35); however, the calculated thickness of the deposited PSU layer agrees excellently with the value obtained for the film before floating from a glass support. The high MSE is probably due to the complexity of the models and limited validity of the assumptions made. In particular, the intrusion layer may in fact comprise PSU, alumina, and remaining void and the assuming identical refractive index for the intrusion region and PSU contentious. Even though, the exponential

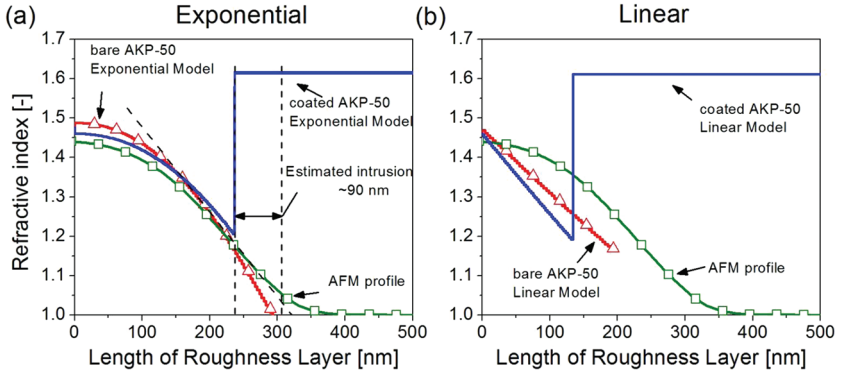

Figure 10. Optical index profile for PSU film deposited on AKP-50 compared with bare AKP-50 (obtained previously) and AFM profiles for exponential and linear profile based models; symbols are guides for the eyes.

dx.doi.org/10.1021/am2015958 | ACS Appl. Mater. Interfaces 2012, 4, 935−943

Table 3. Model Fitting Results for the AKP 50 Coated with PSU Layer at 70° Angle of Incidence and Wavelength Range of 450−1000 nm[a]

	uncoated AKP 50, MSE linear = 1.2, MSE exponential = 2.7					AKP 50 coated with PSU, MSE linear = 35 MSE exponential = 33			
model	thickness of surface layer, h (nm)	mean void fraction in surface layer, v (%)	gradient in the surface layer, g (%)	exponent, e	porosity of the support, p (%)	thickness of PSU layer, h_2 (nm)	thickness of surface layer, h_1 (nm)	mean void fraction in surface layer, v (%)	gradient in the surface layer, g (%)
linear	193.1 ± 1.8	57.0 ± 0.2	62.9 ± 0.7		39.8 ± 0.1	1110.7 ± 1	134 ± 22	55 ± 25	54 ± 11
exponential	336.6 ± 2	76.5 ± 0.1	104.3 ± 1.1	2.16 ± 0.04	38.0 ± 0.6	1109.3 ± 1	181 ± 49	59 ± 3	63 ± 8

[a]For the sample coated with PSU layer, exponent (e) and bulk porosity (p) were held the same as for the uncoated sample.

model seems to represent the curved index AFM profile very well and remains consistent with respect to the index profile of a bare AKP-50 as shown in Figure 10a. On the basis of this model, the thickness of the intrusion region is estimated at about 90 nm.

In the case of the linear model, the refractive index profile shows large deviations from the AFM data and from the modeling results for the bare support. In particular, the slope of the void fraction is too high. Moreover, for the linear model the uncertainties in the fitting parameters are relatively large. The oscillating pattern of psi with wavelength, related to the PSU layer on top of the sample, is captured much less accurately in comparison to the Exponential Model (Figure 11). The reason for the linear model to be less appropriate as compared to the exponential model is the loss of symmetry in the void profile upon addition of the PSU layer. For a bare support, the curvature in void profile at both interfaces is comparable, allowing the linear model to capture the linear variation in void fraction in the middle of the layer. When the PSU layer is added, the curvature in the void space at the interface with the ambient is replaced by an intrusion region, which is accommodated in the PSU layer. The linear model is in this case forced to mimic the curvature at the interface with bulk together with the linear profile adjacent to it. In contrast, the exponential model inherently attempts to capture the curvature at the interface with the bulk. In the case of a bare support, the exponential model fails to describe the curvature in void fraction at the interface with the ambient, which in the multilayer model is replaced by the intrusion region. Consequently, the exponential model appears more appropriate for a support with thin polymer film, as compared to the linear model.

It has to be emphasized that, despite the high MSE, the exponential model is intended primarily to observe changes in thickness and refractive index of the thin polymer layer, under permeation and sorption experiments. Thickness changes are strongly related to the shifts in the oscillating pattern observed both in psi and delta measured data, as shown in Figure 11. It is plausible that the sensitivity to thickness changes is sufficient to obtain meaningful thickness variation data (swelling) in realistic membrane application conditions.

5. CONCLUSIONS

Variable-angle spectroscopic ellipsometry is successfully applied to model polished porous alumina flat discs. Two optical models are designed that consider the surface roughness of these supports as distinct layer, with a porosity profile. The first model considers the porosity profile to be linear; the second model assumes an exponential profile. Density profiles generated by both models are physically realistic and correspond well with atomic force microscopy and mercury porosimetry. The models are extended to accommodate a thin polysulfone film placed on top of the alumina support, representative for a composite membrane. The supported polysulfone layer can be appropriately fit using the exponential model. This indicates that the approach can be used to obtain meaningful information on the in situ swelling behavior of thin dense supported membranes.

AUTHOR INFORMATION

Corresponding Author

*E-mail: n.e.benes@utwente.nl.

Present Address

[⊥]Chemical Process Engineering, RWTH Aachen University, Turmstrasse 46 52064, Germany

ACKNOWLEDGMENTS

The authors acknowledge Michel Klein Gunnewiek for the help with atomic force microscopy analysis and Hammad Qureshi for performing the mercury porosimetry measurements.

REFERENCES

(1) Bertrand, P.; Jonas, A.; Laschewsky, A.; Legras, R. *Macromol. Rapid Commun.* **2000**, *21*, 319−348.

(2) Kawakami, H.; Mikawa, M.; Nagaoka, S. *Macromolecules* **1998**, *31*, 6636−6638.

(3) Wessling, M.; Lidon Lopez, M.; Strathmann, H. *Sep. Purif. Technol.* **2001**, *24*, 223−233.

(4) Ram, M. K.; Yavuz, Ö.; Lahsangah, V.; Aldissi, M. *Sens. Actuators, A* **2005**, *106*, 750−757.

(5) Opila, R. L.; Eng, J. Jr. *Prog. Surf. Sci.* **2002**, *69*, 125−163.

(6) Kamiya, Y.; Mizoguchi, K.; Terada, K.; Fujiwara, Y.; Wang, J. S. *Macromolecules* **1998**, *31*, 472−478.

(7) Wessling, M.; Schoeman, S.; van der Boomgaard, T.; Smolders, C. A. *Gas Sep. Purif.* **1991**, *5*, 222−228.

(8) Simons, K.; Nijmeijer, K.; Sala, J. G.; van der Werf, H.; Benes, N. E.; Dingemans, T. J.; Wessling, M. *Polymer* **2010**, *51*, 3907−3917.

(9) Wormeester, H.; Benes, N. E.; Spijksma, G. I.; Verweij, H.; Poelsema, B. *Thin Solid Films* **2004**, *455−456*, 747−751.

(10) Mattsson, J.; Forrest, J. A.; Börjesson, L. *Phys. Rev. E: Stat., Nonlinear, Soft Matter Phys.* **2000**, *62*, 5187.

(11) Ilton, M.; Qi, D.; Forrest, J. A. *Macromolecules* **2009**, *42*, 6851−6854.

(12) Kamiya, Y.; Mizoguchi, K.; Naito, Y. *J. Polym. Sci., Part B: Polym. Phys.* **1990**, *28*, 1955−1964.

(13) Mapesa, E. U.; Erber, M.; Tress, M.; Eichhorn, K. J.; Serghei, A.; Voit, B.; Kremer, F. *Eur. Phys. J. Special Topics* **2010**, *189*, 173−180.

(14) Stafford, C. M.; Guo, S.; Harrison, C.; Chiang, M. Y. M. *Rev. Sci. Instrum.* **2005**, *76*, 062207.

(15) Soles, C. L.; Douglas, J. F.; Wu, W.-l.; Peng, H.; Gidley, D. W. *Macromolecules* **2004**, *37*, 2890−2900.

(16) Koga, T.; Li, C.; Endoh, M. K.; Narayanan, S.; Lurio, L.; Sinha., S. K. *J. Phys.: Conf. Ser.* **2011**, *272*, 012003.

(17) Benes, N. E.; Spijksma, G.; Verweij, H.; Wormeester, H.; Poelsema, B. *AIChE J.* **2001**, *47*, 1212−1218.

(18) Sirard, S. M.; Green, P. F.; Johnston, K. P. *J. Phys. Chem. B* **2001**, *105*, 766−772.
(19) Madami, M.; Tacchi, S.; Carlotti, G.; Gubbiotti, G.; Stamps, R. L. *Phys. Rev. B: Condens. Matter Mater. Phys.* **2004**, *69*, 144408.
(20) Yang, J.; Liu, C.; Yang, Y.; Zhu, B.; Lee, L. J.; Chen, H.; Jean, Y. C. *J. Polym. Sci., Part B: Polym. Phys.* **2009**, *47*, 1535−1542.
(21) Pham, J. Q.; Johnston, K. P.; Green, P. F. *J. Phys. Chem. B* **2004**, *108*, 3457−3461.
(22) Fujiwara, H. *Spectroscopic Ellipsometry Principles and Applications*; John Wiley & Sons; Chichester, U.K., 2007; p 2.
(23) Tompkins, H. G.; Irene, E. A. *Handbook of Ellipsometry*; William Andrew: Burlington, MA, 2005.
(24) Dong, G.; Li, H.; Chen, V. *J. Membr. Sci.* **2011**, *369*, 206−220.
(25) Visser, T.; Koops, G. H.; Wessling, M. *J. Membr. Sci.* **2005**, *252*, 265−277.
(26) Burggraaf, A. J.; Cot, L. *Fundamentals of Inorganic Membrane Science and Technology*; Elsevier: Amsterdam, 1996; p 119−133.
(27) Nerbo, I. S.; Roy, S. L.; Foldyna, M.; Kildemo, M.; Sondergard, E. *J. Appl. Phys.* **2010**, *108*, 014307.
(28) Lichtenstein, T. *Handbook of Thin Film Materials*; College of Engineering and Applied Science, University of Rochester: Rochester, NY, 1979.